Multipulse photon echoes in $LaF_3:Pr^{3+}$

Lynden E. Erickson
National Research Council, Ottawa, Ontario, Canada K1A 0R8
(Received 23 April 1992)

Multipulse photon echoes are observed from $LaF_3:Pr^{3+}$ and are shown to be primarily stimulated echoes. The various contributions to the echoes were measured using a three-pulse photon-echo sequence that resolved the image of the echo generated by the first two pulses, and the echo generated by the second and third pulses and that of the first and third pulses from the stimulated echo. By use of a theoretical model of Shoemaker [in *Laser and Coherence Spectroscopy,* edited by J. I. Steinfeld (Plenum, New York, 1978)] and relaxation theory of Hu and Hartmann [Phys. Rev. B **9**, 1 (1974)], the image echo contributions to the third echo is shown to be less than 10% of the total for the pulse widths and Rabi frequencies used in the measurements. As a result, multipulse photon echoes will find limited use in measuring coherence decay until very short high-intensity pulses are used to excite the echoes.

PACS number(s): 42.50.Md, 76.60.Es, 78.50.Ec

INTRODUCTION

The NMR community experienced a revolution with the introduction of multipulse NMR to solids by Waugh [1]. This was a result of the large gains in the signal intensity and the resolution attained by suppression of homogeneous broadening in the materials. After Kurnit, Abella, and Hartmann [2] extended NMR coherent transient spectroscopy to the optical regime, a wide variety of coherent optical transient applications were reported. Schmidt, Berman, and Brewer [3] demonstrated infrared multipulse photon echo spectroscopy in studies of NH_3D. Later, Shoemaker [4] provided a model of the coherent optical transients, including multipulse photon echoes in a Doppler-broadened medium. In this he described the various contributors to the echo signal: they include two-pulse echoes from all possible combinations of preceding pulses and the image echoes from a combination of a previous echo and an exciting pulse, all of which are from transverse (T_2) coherence, and the three-pulse (stimulated) echoes resulting from population gratings written by the first two pulses (T_1 effects). He pointed out that if one uses a Carr-Purcell pulse train, with a second pulse angle $\theta_2=\pi$, the stimulated echo, and the two-pulse echoes from all possible combinations of exciting pulse would disappear leaving only the image pulses. In this ideal case, the original coherence is continually refocused and the echo amplitude consists of only contributions from that original coherence. Echo-decay measurements are then valid measurements of the decay of the coherence established by the first pulse.

EXPERIMENT

In an attempt to apply this model to rare-earth optical solids, measurements of multipulse photon echoes were made on $LaF_3:Pr^{3+}$. The exciting light pulses were produced by switching a frequency-stabilized cw dye laser beam (≈ 100 mW) with two acousto-optic (A/O) modulators. The beam was focused, either by a 14.7-cm focal length (FL) lens (multipulse) or by a 7.5-cm FL lens (three pulse), onto the crystal along a direction normal to the c axis. For the 7.5-cm FL lens, the light intensity was approximately 8000 W/cm^{-2} at the 40-μm-diam 0.4-cm-long beam waist. Echoes were detected by optical heterodyne detection of the A/O gated echoes (with the unshifted light) on a photodiode followed by a preamplifier, a 30-MHz intermediate-frequency (IF) amplifier, diode video detector, and a digital oscilloscope. The signals were averaged over 256 repeated pulse sequences. The repetition rate was usually 3 Hz, but the results were independent of the repetition rate to 0.1 Hz [5]. In this configuration, echo *intensity* and not *amplitude* was observed. The phase stability of the Mach-Zehnder interferometer formed by the optical heterodyne scheme was inadequate for use of a rf homodyne mixer (to downshift the 30-MHz echo to dc) and thereby observe the echo *amplitude* and *phase.* A 1-mm-diam aperture was placed in front of the photodiode detector to sample only the central part of the beam to reduce effects of spacial variation of light intensity on the echo response. The echo signal at 30 MHz is derived from the optical frequency offset produced by the two-pulse forming A/O modulators (80 MHz+90 MHz), and an additional shift of -200 MHz by the gate A/O modulator preceding the detector. The $LaF_3:Pr^{3+}$ (0.1 at. %) sample was held at 2 K either in liquid helium or with the helium level just below the sample. Two-pulse photon-echo lifetimes T_2 were observed to be 5.64 and 21.5 μs for a static magnetic field of 0 and 80 G applied to the sample, respectively. These agree with previously published values [6].

The multipulse sequences used all have a preparation pulse at one-half the cycle time τ_c prior to the second pulse. The second and succeeding pulses are either the same length as the first pulse (spin-lock) or twice the length of the first pulse (Carr-Purcell) [7]. A typical spin-lock multipulse train is shown in Fig. 1 and a plot of echo peak intensity versus time is shown in Fig. 2. Photon echoes were observed with lifetimes as long as 100 μs. The lifetime was independent of cycle time, but became

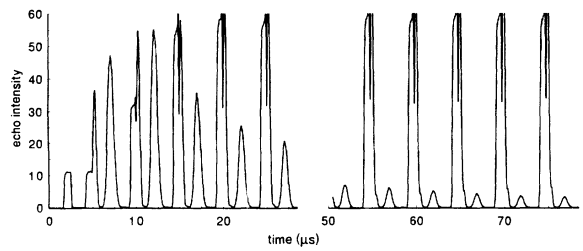

FIG. 1. A spin-lock multipulse photon-echo train is shown for a pulse width of $\tau_{pi}=0.89$ μs and a pulse period (cycle time) $\tau_c=4.98$ μs in the absence of a static magnetic field. The sample, at 2 K, was illuminated perpendicular to the crystal c axis. The echo pulses, clearly seen between the exciting pulses, show an amplitude-decay time $\tau_d=60$ μs. The structure on the right-hand side of the exciting pulse is due to leakage through the switching transient of the acousto-optic modulator used to protect the detector from the full force of the exciting light.

longer with shorter (smaller angle) exciting pulses. Except for the first few pulses the echo decay time was independent of the external field (either 0 or 80 G). The echo intensity was largest with an external field and with the shortest cycle time. For a coherence T_2 process the lifetime should increase by at least a factor of 4 when the magnetic field is changed from 0 to 80 G. Also, if the NMR experience is transferable to photon echoes, the lifetime should decrease with increasing cycle time τ_c ($\propto\tau^{-2}$ to τ^{-5}) [8]. These multipulse echoes would seem to possess very little transverse coherence (T_2). Similar results were obtained from Carr-Purcell pulse trains.

The relative size of various components of the second and succeeding echoes of the pulse train were measured using a three-pulse echo sequence shown in Fig. 3(a). The pulse timing was chosen so that each of the components are resolved in time. A typical measurement is shown in Fig. 3(b). The leakage of the exciting pulses mark their locations. There are four echo components formed, two of which contribute to the second multipulse echo. The first is the stimulated echo. The second is the image of

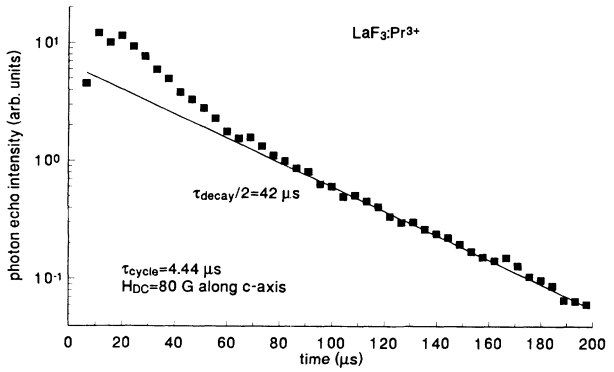

FIG. 2. The decay of spin-lock multipulse photon-echo intensity is shown, using the same pulse sequence as Fig. 1 but with the crystal in a static magnetic field of 80 G. The decay consists of two parts, initially a faster component, and at longer times, an exponential decay of the echo amplitude at a 84-μs rate.

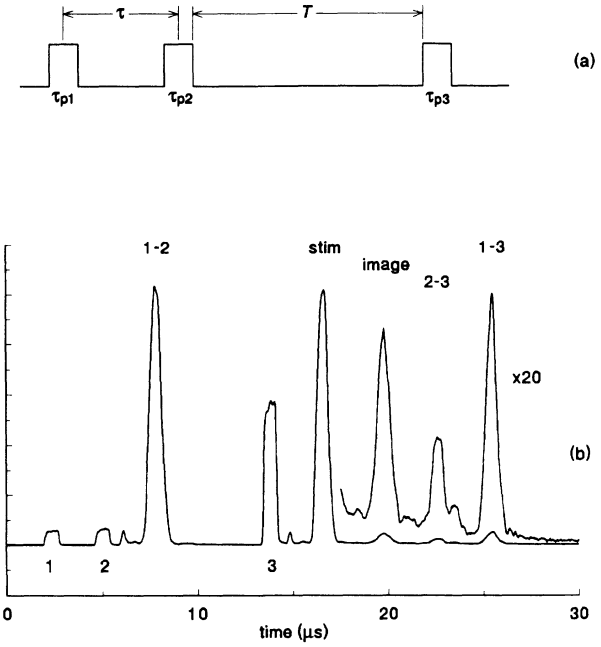

FIG. 3. (a) The pulse sequence used to measure the individual components of the three-pulse-induced photon echo; (b) a typical measurement of the resolved three-pulse-induced echoes for a pulse width $\tau_{p1}=0.78$ μs, $\tau=2.67$ μs, and $T=8.0$ μs. The various components are labeled to indicate their origins; *stim* indicates the usual three-pulse stimulated echo, *image* is the two-pulse echo formed by the first two pulses recreated by the third pulse, and *2-3* is a two-pulse echo that is created by the second exciting pulse and the third exciting pulse.

the first echo formed by the third exciting pulse. Following are the echoes formed by the second and third exciting pulses (2-3 echo) and that formed by the first and third exciting pulses (1-3 echo). The (1-2) two-pulse echo and the three-pulse stimulated echo are about 20 times larger than the image and the 2-3 and 1-3 echoes. In the absence of coherence (T_2) decay, the components are expected to be about the same size. From the Hu-Hartmann theory [9] of echo decay and the experimental data from Shelby, Yannoni, and Macfarlane [10] the echo intensities are calculated to be reduced by coherence decay; during the 11.72 μs between the first echo and the image, its *intensity* is multiplied by a factor 0.48. Similarly, for the 2-3 echo (17.06 μs) and the 1-3 echo (22.39 μs) the intensity is 0.32 and 0.22 of the intensity that one would observe if T_2 was much larger than the time of the experiment. The stimulated echo intensity is also expected to be multiplied by a factor 0.83 due to T_2 relaxation (Ref. [9]). Measurements of these four echo intensities as a function of the pulse angle were made for both the three equal pulse sequence (spin-lock, pulse angles $\theta_1=\theta_2=\theta_3$) and a sequence where the first pulse angle θ_1 is one-half the angle of the other two pulses (Carr-Purcell). The pulse-angle variation was obtained using fixed optical power and by varying the first pulse width from about 0.3 to 1.2 μs. The time between the centers of

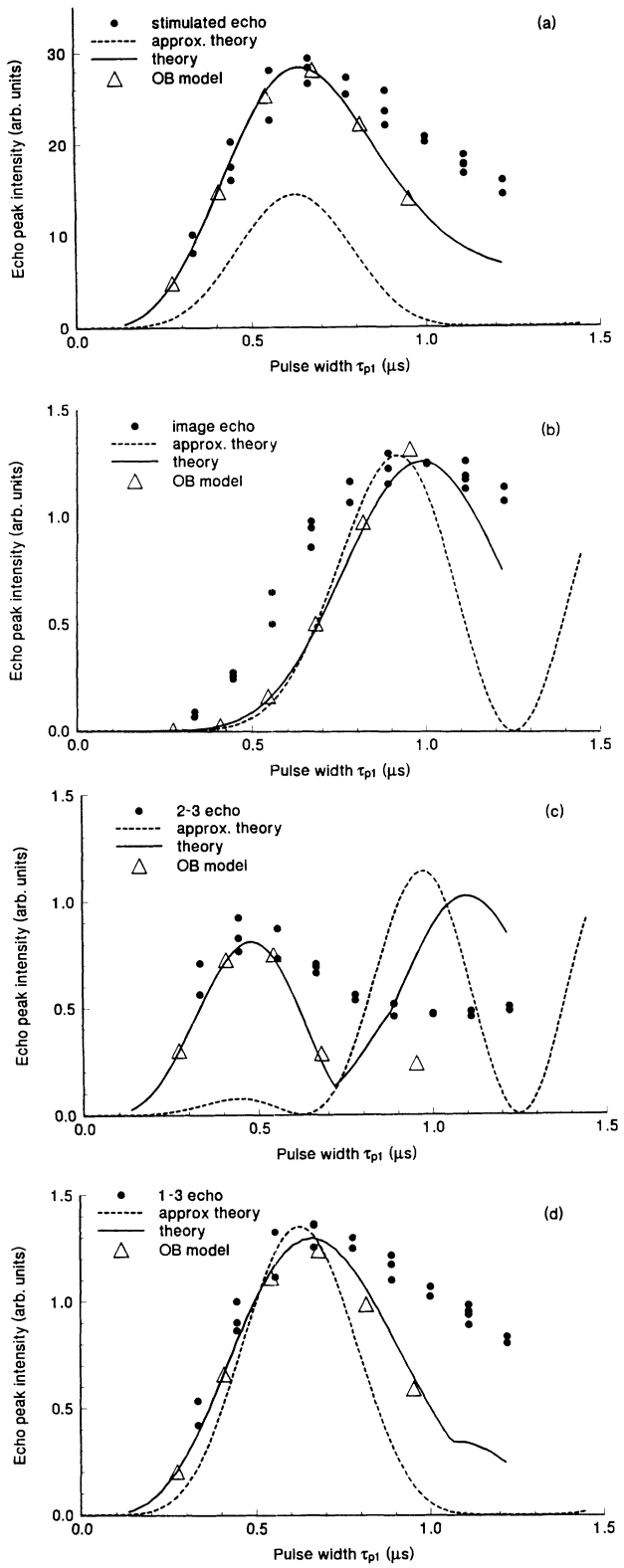

FIG. 4. The measured intensities of the photon-echo components for a three-pulse spin-lock sequence ($\tau=2.67$ μs, $T=8.0$ μs) are plotted as a function of the pulse width τ_{p1} for the (a) stimulated echo, (b) the image echo, (c) the 2-3 echo, and the (d) 1-3 echo. These are compared to an approximate theory (dashed line) and a more exact theory (solid line). The triangles are calculated using an optical Bloch model which includes both coherence (T_2) and population (T_1) decay throughout.

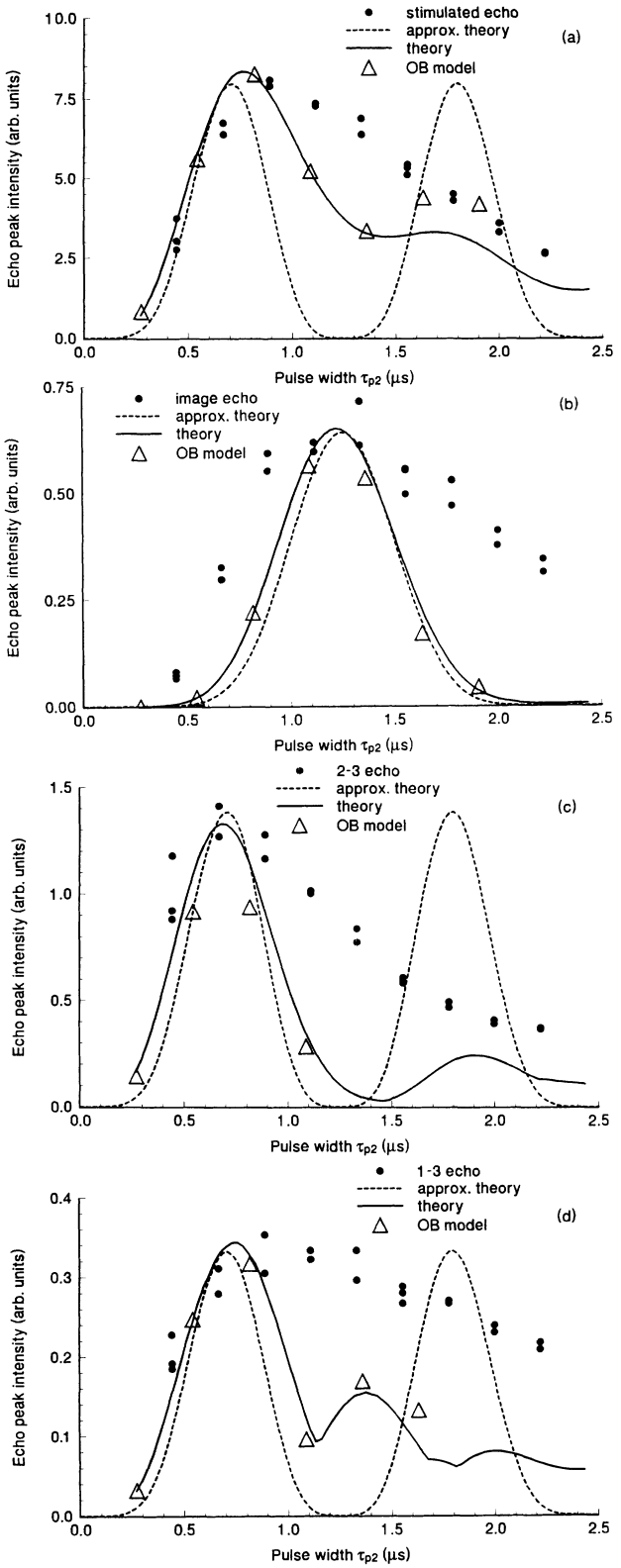

FIG. 5. The measured intensities of the photon-echo components for a three-pulse Carr-Purcell sequence ($\tau=2.67$ μs, $T=8.0$ μs) are plotted as a function of the pulse width τ_{p2} for the (a) stimulated echo, (b) the image echo, (c) the 2-3 echo, and the (d) 1-3 echo. These are compared to an approximate theory (dashed line) and a more exact theory (solid line). The triangles are calculated using an optical Bloch model which includes both coherence (T_2) and population (T_1) decay throughout.

the first two pulses is fixed at $\tau=2.67$ μs, and the time from the end of the second pulse to the beginning of the third pulse is fixed at $T=8$ μs. The sample was at 2 K and in a static magnetic field of 80 G. Plots of the spin-lock echo intensities versus pulse length $\tau_{\rm pl}$ are shown in Figs. 4(a)–4(d), and the Carr-Purcell data are shown versus τ_{p2} in Figs. 5(a)–5(d). There are two lines superimposed on the measurements. The solid lines will be discussed later. The dashed lines, labeled *approx. theory* on the curves, are derived from the theory that Shoemaker (Ref. [4], Eqs. 3-164 and 3-180) developed for free collisionless molecules. The model was constructed with the hypothesis that the exciting light is so intense that $\kappa E_0 \gg k\bar{u}$, where $\kappa E_0=\mu_{ab}E_0/\hbar$ is the transition amplitude (Rabi frequency), k is the number of waves per unit length, and $\bar{u}$ the most probable speed in a Gaussian distribution of velocities in a gas. The value of $k\bar{u}$ is the linewidth of the Doppler-broadened spectral line. The equivalent linewidth for a solid is the inhomogeneous (strain and dislocation) broadening of the spectral line. If the inequality is satisfied, the whole spectral line is illuminated by the broad spectral width of short pulse. His equations for the echo intensities are reproduced here for the convenience of the reader:

$$I_{\text{two pulse}}(\theta_1,\theta_2)=C_{\text{two pulse}}(t,\tau)[\sin\theta_1(1-\cos\theta_2)]^2 , \quad (1)$$

$$I_{\text{stimulated}}(\theta_1,\theta_2,\theta_3)=C_{\text{stimulated}}(t,\tau,T)[\sin\theta_1\sin\theta_2\sin\theta_3]^2 , \quad (2)$$

$$I_{\text{image}}(\theta_1,\theta_2,\theta_3)=C_{\text{image}}(t,\tau,T) \times[\sin\theta_1(1-\cos\theta_2)(1-\cos\theta_3)]^2 , \quad (3)$$

$$I_{2\text{-}3}(\theta_1,\theta_2,\theta_3)=C_{2\text{-}3}(t,\tau,T)[\cos\theta_1\sin\theta_2(1-\cos\theta_3)]^2 , \quad (4)$$

$$I_{1\text{-}3}(\theta_1,\theta_2,\theta_3)=C_{1\text{-}3}(t,\tau,T)[\sin\theta_1(1+\cos\theta_2)(1-\cos\theta_3)]^2 . \quad (5)$$

The pulse angles are $\theta_i=\kappa E_0\tau_{pi}$ $(i=1,2,3)$. In the absence of relaxation, the constants C are equal for Eqs. (2)–(5). By inspection, one observes for a second pulse angle $\theta_2=\pi$, the stimulated echo, the 1-3 echo, and the 2-3 echo disappear leaving only the image echo (if $\theta_1\neq\pi$). This is the only situation for which the image echo is dominant over the other components. The experimental three-pulse spin-lock data in Fig. 4 show that the stimulated echo is about 25 times larger than the image echo. For small pulse angles, the theory and experiment are in approximate agreement for the 1-2 two-pulse (not shown), 1-3 two-pulse, and the stimulated echoes, but the observed image echo is larger than expected. The measured and the calculated 2-3 two-pulses echo differ markedly. As the pulse angle increases, the agreement between this approximate theory and the measured echoes becomes less satisfactory. For the Carr-Purcell three-pulse echo data of Figs. 5, the small-angle calculations show general agreement with the measured data for both the stimulated and 1-3 echoes, and the measured image echo is generally larger than one would expect from this theory. However, small-angle data for the 2-3 echo now show some agreement with this approximate theory. One notes that none of the measured echoes reaches zero amplitude with a second-pulse angle $\theta_2=\pi$, and for longer pulses the differences become even larger. The reason for this discrepancy is that the optical power is insufficient to satisfy the inequality $\kappa E_0 \gg k\bar{u}$ assumed in deriving Eqs. (1)–(5). Since the inhomogeneous width of the $^3H_4\rightarrow{}^1D_2$ (16873.1 cm^{-1}) transition in LaF_3:Pr^{3+} is about 2 GHz, π pulse widths less than 0.1 ns would be needed. For the opposite limit $\kappa E_0 \ll k\bar{u}$, the entire optical line is not illuminated because the spectral width of the long optical pulse is less than the optical linewidth. A more general calculation in this limit has been outlined by Shoemaker [4]. A two-dimensional representation is used to describe the behavior of the two optical levels excited by a series of pulses. The Bloch u, v, and w spin parameters are written as

$$\mathbf{m}=\begin{pmatrix} w & u-iv \\ u+iv & -w \end{pmatrix} . \quad (6)$$

In this representation the total rotation is written as

$$\mathbf{m}'=\mathbf{r}_T\mathbf{m}\mathbf{r}_T^{-1} , \quad (7)$$

where the transformation $\mathbf{r}_T$ is given by the product of transformations $\mathbf{r}$, one for each light pulse and one for the time between each of the exciting pulses,

$$\mathbf{r}_T=\begin{pmatrix} \alpha & \beta \\ -\beta^* & \alpha^* \end{pmatrix}=\prod_{n=1}^{N}\begin{pmatrix} \alpha_n & \beta_n \\ -\beta_n^* & \alpha_n^* \end{pmatrix} . \quad (8)$$

Here during the exciting pulse

$$\alpha_n=\cos(g\tau_{pn}/2)-i\frac{\delta}{g}\sin(g\tau_{pn}/2) , \quad (9)$$

$$\beta_n=-i\frac{\kappa E_0}{g}\sin(g\tau_{pn}/2) \quad (10)$$

and between the pulses

$$\alpha_n=\exp(\pm i\delta t/2), \quad \beta_n=0 . \quad (11)$$

In Eqs. (9) and (10)

$$g=[(\kappa E_0)^2+(\Omega-\omega_0)^2]^{1/2} , \quad (12)$$

and in Eq. (11), $\delta=\Omega-\omega_0$ is the offset of the resonant (optical) frequency of the ion from the excitation (optical) frequency. The pulse angle $\theta_i=g\tau_{pi}$. The echo amplitude is given by

$$v=2c\int_{-\infty}^{\infty}\text{Im}(\alpha\beta)d\delta , \quad (13)$$

where the integration is over the inhomogeneous spectral line. c is a constant.

This formalism was used to compute the stimulated echo, image echo, 2-3 echo, and the 1-3 echo for a fixed Rabi frequency and optical pulse lengths typical of the measurements. A typical calculation of the spin-lock and Carr-Purcell echoes is given in Fig. 6 for a first pulse angle $\theta_1=\pi/2$ ($\tau_{p1}=0.68$ μs). The spin-lock result is straightforward, with clearly resolved echoes as are ob-

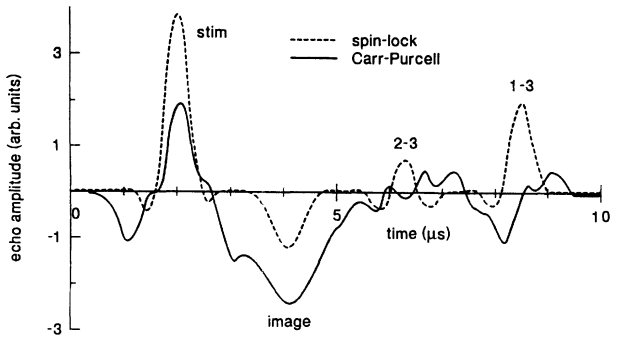

FIG. 6. A typical calculation of the echo amplitudes produced by the first three pulses of a modified spin-lock (dotted) and Carr-Purcell (solid line) sequence for pulse widths and separations typical of these experiments. The pulse angle $\theta_1=\pi/2$ corresponds to a pulse width $\tau_{p1}=0.68$ μs in Fig. 5. The time origin is at the end of the third pulse for the spin-lock sequence. The Carr-Purcell time origin has been offset because the third-pulse width is 2× the spin-lock case. The free induction decay (FID) term after the third pulse has been suppressed.

served in Fig. 3(b). The Carr-Purcell result is more complex. The stimulated and image echoes are unambiguous. The 2-3 and the 1-3 echoes have a structure which makes comparison of theory with experiment more difficult. The Shoemaker approximate theory takes the amplitude at the precise time of the echo. One can measure this if that time is known precisely. This yields a much smaller value for the 2-3 echo and the 1-3 echo for $\theta_1=\pi/2$ than the maximum intensity in the vicinity of the expected echo time as is used in these experiments. This accounts for much of the difference between the approximate theory and the curves labeled theory in Figs. 4 and 5 for the 2-3 and 1-3 echoes. The echoes were calculated for a fixed Rabi frequency and varying pulse widths. The value plotted in Figs. 4 and 5, for each component and each angle, is the maximum value of the *intensity* for the term calculated separately. For small angles, this does not differ from the calculation which includes all four terms simultaneously, but for larger angles where echoes begin to overlap, small differences are seen for the 2-3 echoes. Because the echo shapes for large angles are structured, the separate calculation provided an unambiguous identification of echo signal. One sees discontinuities in the intensity curves versus angle because another part of the echo structure becomes largest as the pulse angle is changed. The horizontal and vertical scale factors were chosen to give a reasonable approximation to the *stimulated echo* for small pulse widths for the two cases. The effective Rabi frequency $\kappa E_0=400$ kHz. Only the vertical scale factors were adjusted for the other components. The relative (to the stimulated echo) vertical scale factors are given in columns (3) and (4) of Table I together with the estimated correction factor to account for coherence decay in column (2). The theory gives equal values in each column in the absence of coherence decay. The measured values, corrected for coherence decay, for the 2-3 echoes and the 1-3 echoes are approximately 0.78 and 0.65 times the stimulated echoes, for the spin-lock and Carr-Purcell cases, but the measured image echo is only 0.27 times the stimulated echoes for the spin-lock case and 0.20 times for the Carr-Purcell measurement. Since this theory does not include relaxation explicitly, and the relaxation is superimposed, the agreement is quite satisfactory.

There is some improvement in the fit of this theory to the spin-lock data, compared to the fit of the approximate theory [Eqs. (1)–(5)] for larger times. For the 2-3 echo, the small-angle calculations are greatly improved over the approximate theory, but the large-angle results still differ markedly from the calculated curve. The reason for this is not fully understood, but it is thought to be due to the (phase) fluctuations which are observed in photon-echo experiments, and to nonuniformities in the optical-field strength along the length of the crystal. The fluctuations from one pulse sequence to the next causes echo intensities to vary by up to a factor of 2. Part of this instability is due to the Mach-Zehnder interferometer used for the optical heterodyne detection. The fit of the theory to the Carr-Purcell data shows an improvement for all of the echo components except the image echo where one observes the same characteristics as in the spin-lock case: a larger amplitude at small (pulse) angles than expected, and poor agreement at large pulse widths (angles).

On revisiting Fig. 1, the decay corrections are different from those in Table I because the times are now different.

TABLE I. The constants for the Shoemaker theory [Eqs. (6)–(11)] used to obtain the solid lines on Figs. 4 and 5 are given in the third and fourth columns. In comparing these constants to the expected equal values in the spin-lock and Carr-Purcell columns, one must take into account the decay of the stimulated echo and the two-pulse echo intensities during the measurement period. This was done by dividing the measured photon-echo components by an intensity decay correction (second column) obtained using the Hu-Hartmann theory of echo decay (Ref. [9]) and the measured coherence lifetimes (Ref. [10]). The coherence decay due to the upper state is ignored because it is much smaller; the nuclear moment is not enhanced in the upper state. The values of the third and fourth columns, normalized by the Hu-Hartmann decay corrections, are shown in parentheses, and those normalized by the optical Bloch decay corrections are shown in brackets in the same columns.

Intensity constant	Decay correction	Spin-lock	Carr-Purcell
$C_{\text{stimulated}}$	0.83	1.00 (1.0) [1.0]	1.00 (1.0) [1.0]
C_{image}	0.48	0.157 (0.27) [0.43]	0.116 (0.20) [0.34]
$C_{2\text{-}3}$	0.32	0.300 (0.78) [0.80]	0.301 (0.78)
$C_{1\text{-}3}$	0.22	0.176 (0.66) [0.83]	0.172 (0.65) [0.73]

For the stimulated echo $\tau=\tau_c/2$, $T=\tau_c-\tau_{p2}$, the image time is τ_c, and the 2-3 and 1-3 echoes decay over $2\tau_c$ and $3\tau_c$. The amplitude corrections are 0.92,0.90,0.75,0.59 for the stimulated, image, 2-3 and 1-3 echoes, respectively. The calculated echo amplitude maxima, not corrected for coherence decay ($\theta_1=0.32\pi$), are 1.0, −0.12, 0.38, and 0.50. One concludes from this analysis that the observation of the stimulated echolike character of the observed multipulse echoes is correct, but that the image contribution for the second echo could reduce the total amplitude by about 12% and increase the third echo amplitude by about 9% [11]. The third echo also has a 1-3 component which could add 30%. If one introduces another factor for the observed size of the image compared to the calculation, the influence of the image on the observed multipulse echo amplitude is reduced by a factor 2.5 to a value of 5%. No such effect is observed in Figs. 1 or 2.

DISCUSSION

In the long-pulse regime of these experiments, any coherence relaxation which occurs during the optical pulses will modify the echo amplitudes. This is a concern because the Shoemaker model used in this paper does not include relaxation and the Hu-Hartmann relaxation model which was superposed on it assumes δ-function excitation pulses. Intuitively, for pulse lengths about 1 μs and $T_2=21$ μs, one would expect that the effect of relaxation during the excitation pulses would be small. A conventional optical Bloch (OB) model [12], which includes both population (T_1) and spin coherence (T_2) relaxation, was used to calculate the effect of pulse width on the amplitudes of the various echo components. These calculations were made for first pulse angles ($\theta_1=\pi/2$) and for several values of the Rabi frequency corresponding to a change in pulse length by a factor of 5. The amplitude-decay corrections for the echo components are given in Table II for both the spin-lock and Carr-Purcell pulse sequences and three values of the Rabi frequency. One notes immediately that the decay corrections differ from those obtained by the Hu-Hartmann model; the OB model shows a greater decay than the Hu-Hartmann model. Additionally, the two sequences have virtually identical OB decay corrections, and the fivefold reduction of the pulse length only slightly modifies the ratio of the amplitudes. In columns 3 and 4 of Table I, the numbers in brackets give the ratio of the observed intensities to the OB model predictions. A good fit would give unity for all of the values in parenthesis and/or brackets. OB calculations versus the pulse area for a fixed Rabi frequency of 400 kHz also show that these ratios are independent of pulse area for the pulse lengths used in these experiments. This lack of pulse-angle dependence is demonstrated by plotting a few points obtained with the OB model in Figs. 4 and 5. These are shown as triangles on the figures, scaled by the numbers in brackets in Table I. In most cases they lie on the solid lines calculated using Eqs. (6)–(13). One would conclude from these calculations that relaxation during the excitation does not have a different influence on the result than that during the field-free regions. And that for these experiments, the relaxation can be accommodated by a simple scale factor. The OB decay gives improved results over the combined Shoemaker and Hu-Hartmann theory in calculating this scale factor for the image echo, but neither model fits the observed image echo nor is accurate for large-pulse angles.

As the pulse length θ_i approaches $\pi/2$, the emitted stimulated, 1-3, and 2-3 echo patterns become structured with widths similar to the exciting pulse widths τ_{pi}. If the various components are not well time resolved, interference between components where they overlap makes the already complex components even more complex. On calculating the echo response from $\theta_1=\pi/2$ pulses 1000× shorter in time, one observes that the stimulated echo reaches zero amplitude twice, but that there is a significant nonzero amplitude in the immediate vicinity. This amplitude is about −0.64× the calculated image echo. The 1-3 echo is about 0.32× the image echo, and will add to the image on the subsequent echo. The peak 2-3 echo amplitude is −0.06× the image echo (a zero crossing at center of pattern), but it occurs at the time of the next exciting pulse if strict Carr-Purcell timing is used, so it will *not* contribute directly to the multipulse echoes. Even with this 1000× narrower pulse width (time), the calculated echo does not approach the ideal picture outlined by Shoemaker. It seems that the inverse of the optical pulse width (time) must be short compared to (inhomogeneous optical linewidth)/π and

TABLE II. The effect of relaxation during the pulse sequence on the echo amplitudes as a function of the Rabi frequency (kHz) for a fixed first pulse angle $\theta_1=\pi/2$. These factors were calculated using the optical Bloch model with $T_1=500$ μs and $T_2=21.4$ μs. Since the correction factors show little dependence on the Rabi frequency (i.e., inverse pulse width), this table demonstrates that the pulse width is not responsible for the discrepancies between the experiment and the Shoemaker model. The amplitude-decay factors calculated using the Hu-Hartmann model, which are used in Table I, are given on the line labeled H-H. The optical Bloch model indicates a greater decay than the Hu-Hartmann model.

Rabi	Spin-lock				Carr-Purcell		
Freq.	stim	image	2-3	1-3	stim	image	1-3
400	0.767	0.464	0.470	0.354	0.754	0.443	0.367
1000	0.767	0.471	0.472	0.366	0.761	0.464	0.372
2000	0.769	0.474	0.474	0.370	0.764	0.470	0.371
H-H	0.91	0.69	0.56	0.47	0.91	0.69	0.47

that the amplitude sample time must be short compared to the optical pulse width to suppress the stimulated echo. This is more difficult for a solid than for a Doppler-broadened medium. The use of multipulse photon echoes to study dephasing in rare-earth optical materials will require much larger Rabi frequencies (κE_0) than are used in these experiments. This will allow much shorter cycle times, and will yield some of the benefits of lengthened coherence decay seen in NMR [8]. These can be achieved by using brute force (high-peak-power picosecond lasers) to increase E_0 or by choice of a material where the optical-absorption coefficient is much larger, which increases κ. Because the intensities of a given transition are largely determined by selection rules (symmetry), choosing a different host can strongly affect the optical absorption. One example is $YAlO_3:Pr^{3+}$, where the optical absorption is about ten times larger. Unfortunately, for this material, only part of the absorption increase is due to selection rule changes, so the population decay time T_1 is reduced from 520 μs of $LaF_3:Pr^{3+}$ to 180 μs. Also the $\pi/2$ pulse is still much too long (time) to illuminate the entire inhomogeneous optical line.

CONCLUSION

Multipulse photon echoes have been observed from Pr^{3+} in LaF_3. The observed echoes are shown to be primarily stimulated echoes with the images of the previous echo representing less than 12% of the stimulated echo (when corrected for the T_2 decay during the experiment). The observed image echo for both the spin-lock and the Carr-Purcell sequence is much smaller than one would expect from the theory, and the other two-pulse (T_2) contributors to the multipulse echo are not negligible for the pulse lengths used in this study. Measurements of multipulse photon echoes in optical solids will not provide reliable coherence-decay information until much shorter pulses, which excite the entire inhomogeneous optical width, are used to generate the echoes.

ACKNOWLEDGMENTS

I wish to thank A. Szabo for many useful discussions during the course of this work, and for providing the optical Bloch model computer program, and J. Froemel for technical assistance.

[1] E. D. Ostroff and J. S. Waugh, Phys. Rev. Lett. **16**, 1097 (1966); J. S. Waugh, L. M. Huber, and U. Haeberlen, *ibid.* **20**, 180 (1968).

[2] N. A. Kurnit, I. D. Abella, and S. R. Hartmann, Phys. Rev. Lett. **13**, 567 (1964).

[3] J. Schmidt, P. R. Berman, and R. G. Brewer, Phys. Rev. Lett. **31**, 1103 (1973).

[4] R. L. Shoemaker, in *Laser and Coherence Spectroscopy*, edited by J. I. Steinfeld (Plenum, New York, 1978), p. 197.

[5] The exciting laser frequency was swept slowly (500 MHz/s) to avoid saturation due to the long ground-state hyperfine lifetime (T_1) at these temperatures.

[6] R. M. Macfarlane, R. M. Shelby, and R. L. Shoemaker, Phys. Rev. Lett. **43**, 1726 (1979); S. C. Rand, A. Wokaun, R. G. DeVoe, and R. G. Brewer, *ibid.* **43**, 1868 (1979).

[7] The NMR nomenclature is used here.

[8] W. K. Rhim, D. D. Elleman, and R. W. Vaughan, J. Chem. Phys. **59**, 3740 (1973); R. A. Marino, and S. M. Klainer, *ibid.* **67**, 3388 (1977).

[9] P. Hu and S. R. Hartmann, Phys. Rev. B **9**, 1 (1974).

[10] R. M. Shelby, C. S. Yannoni, and R. M. Macfarlane, Phys. Rev. Lett. **41**, 1739 (1978).

[11] The only way to get a correct value for the echo is to include all of the terms in the calculation. Thus for the third echo, another two terms would be included in Eq. (8) for the field-free period between the third and fourth pulses, and for the fourth pulse.

[12] A. Szabo and T. Muramoto, Phys. Rev. A **37**, 4040 (1988).